Korean J. Chem. Eng., 33(9), 2555-2566 (2016)
DOI: 10.1007/s11814-016-0125-3

pISSN: 0256-1115
eISSN: 1975-7220

C_2H_6/CO_2 oxidative dehydrogenation (ODH) reaction on nanostructured CrAPSO-34 catalyst: One-pot hydrothermal vs. conventional hydrothermal/impregnation catalyst synthesis

Farhad Rahmani*, and Mohammad Haghighi*,**,†**

*Chemical Engineering Faculty, Sahand University of Technology, P. O. Box 51335-1996, Sahand New Town, Tabriz, Iran
**Reactor and Catalysis Research Center (RCRC), Sahand University of Technology,
P. O. Box 51335-1996, Sahand New Town, Tabriz, Iran
(*Received 29 January 2016 • accepted 2 May 2016*)

Abstract−A series of Cr incorporated SAPO-34 catalysts varying in Cr content and a Cr supported SAPO-34 catalyst were prepared by one-pot hydrothermal and incipient-wetness impregnation methods, respectively. The synthesized materials were characterized by XRD, FESEM, TEM, BET, EDX dot mapping, TPD-NH_3 and FTIR, and tested in ethane dehydrogenation with CO_2 reaction. The incorporation of Cr^{3+} into the SAPO-34 framework and impregnation of Cr species were proved by TEM technique. With increase in the incorporated Cr content, smaller cubic crystals and amorphous particles were obtained. However, the extra-framework species probably appeared. Chromium impregnation led to micropore blockage and surface coverage partly, resulting in morphology change somewhat, significant decrease of surface area and acidity as evidenced by FESEM, TEM, BET and TPD-NH_3 analysis. However, one-pot synthesis not only preserved the structure of SAPO-34 but also allowed higher surface area, more effective surface acidity and better chromium dispersion to be achieved, features that account for superior catalytic performance and stability of directly synthesized Cr rich catalyst. The Cr incorporated SAPO-34 catalyst containing rich amount of Cr exhibited the best catalytic activity, showing 38% ethylene yield at 700 °C even after 5 h on-stream operation.

Keywords: CrAPSO-34, One-pot Hydrothermal, C_2H_6/CO_2 Oxidative Dehydrogenation, Ethane, Ethylene

INTRODUCTION

The development of efficient catalysts for selective functionalization of alkanes is one of the primary goals of the petrochemical industry [1]. Extensive works have investigated the catalytic oxidation process, especially for ethylene production, using the CO_2-assisted dehydrogenation of ethane route [2-10]. Supported chromium oxide (CrO_x) catalysts have been intensively investigated because of their good performance [11-14]. Nevertheless, their performance is still insufficient for industrial application. Catalytic performance of chromium-based catalysts depends mainly on support and deposition method. The support itself violently affects the catalytic performance of Cr-based catalysts. It has influence not only on the dispersion of Cr species [14-16], but also on the nature of active sites (reactivity, acidity, accessibility, etc.) [16,17]. The textural properties and acid-base character of the support are the most important factors [16,18]. Acidity is essential; however strong acidity favors the successive formation of oxygenated products [19]. Accordingly, weak to medium acid sites are favorable. On the other hand, the surface area of support affects the metal dispersion. The high-surface-area supports, facilitating good dispersion of CrO_X species, provide more high-valent and reducible chromium species, which are believed to be the active sites or the precursors of the active sites [5,14]. Considering these aspects, the use of SAPO-34 as support seems to be advantageous for oxidative dehydrogenation of alkanes because of high surface area and moderate acidity. SAPO-34 is an acid silico-aluminophosphate with chabasite-related structure where the access to the micropores is limited by eight-membered rings. As reported [20,21], SAPO-34 is a promising catalyst for ethane ODH reaction, exhibiting very interesting catalytic performances which are related to contribution of both Lewis and Brønsted acid sites. Therefore, studies of chromium species dispersed over SAPO-34 would be useful in developing Cr-containing catalysts with desirable catalytic activities for ethane dehydrogenation.

The deposition method of the active chromium phase strongly affects the nature and abundance of CrO_X species. The wet impregnation method is very often used for the deposition of CrO_X species [2,3,6-8,10,12-14,22,23]. However, the impregnation method very often results in broad distribution of Cr species containing the CrO_X units with a low degree of dispersion or bulk oxide [16]. Moreover, these post-synthetic methods sometimes lead to channels blockage by the formation of bulk metal oxide clusters [16,24], especially in the case of SAPO-34 materials. Although the restricted space of zeolitic cages may play a decisive role for enhancing the selectivity to light alkenes, it reinforces the possibility of pores and channels blockage by active metal clusters, and hence restricts attainable chromium loading. The synthetic complication related to multiple synthesis and calcination steps is another disadvantage of these methods. These problems could be overcome using direct or

†To whom correspondence should be addressed.
E-mail: haghighi@sut.ac.ir

one-pot synthesis method. Surfaces with larger surface area, well-dispersed and more reducible catalytic species; and no blocking of pores are made possible using one-pot synthesis. Materials prepared in this way offer superior catalytic performance in oxidative dehydrogenation reaction [4,16,17,24]. An alternative route for the chromium species deposition over the SAPO-34 is the Cr incorporation into the SAPO-34 framework via direct hydrothermal synthesis in which the required amount of proper metal salts is introduced to the synthesis gel. Some attempts have been made to incorporate chromium metal into the SAPO framework directly [25,26]. However, none of them have been employed in the ODH process.

In this communication, a series of Cr incorporated SAPO-34 composites were prepared with various Cr content by one-pot hydrothermal method. The obtained materials were characterized with various physicochemical techniques and examined their catalytic performance as the catalysts for the ethane dehydrogenation in the presence of CO_2. To gain a more detailed insight into the effect of directly Cr deposition, Cr supported SAPO-34 sample was also synthesized by conventional wet impregnation method and compared as for catalytic behavior and physicochemical characteristics to Cr incorporated SAPO-34 catalysts.

MATERIALS AND METHODS

1. Materials

The reagents used for the preparation of SAPO-34-based samples were aluminum isopropoxide (Aldrich, 98+ %), fumed silica

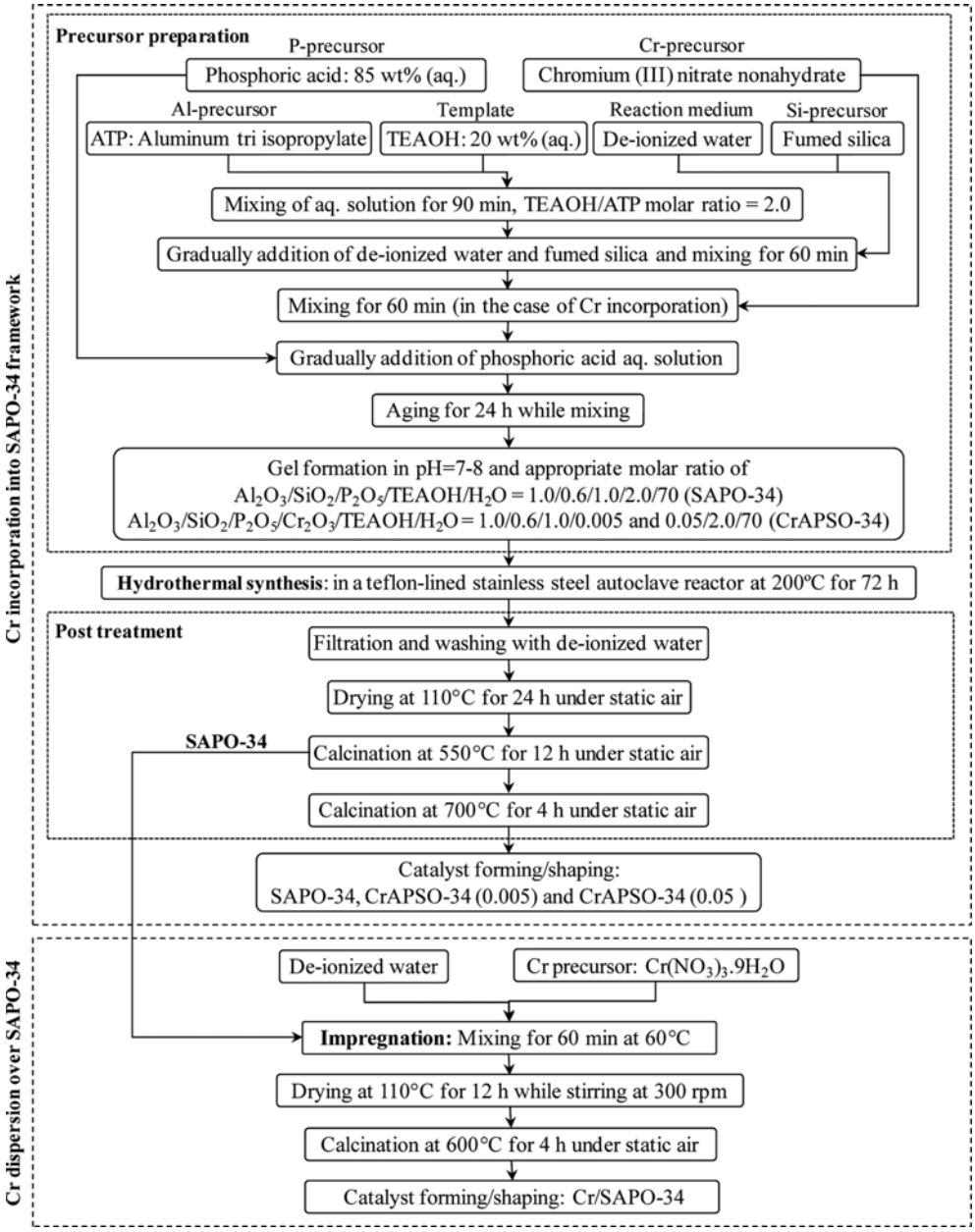

Fig. 1. Synthesis steps of nanostructured catalysts: SAPO-34, CrAPSO-34(0.005), CrAPSO-34(0.05) and Cr/SAPO-34.

(Aldrich, 99.9%), phosphoric acid (Merck, 85%) and chromium nitrate nonahydrate (Chem-Lab, 96%) as the sources of Al, Si, P and Cr, respectively. TEAOH (Aldrich, 20%) was used as the structure-directing agent (SDA). All chemicals were used as received without further treatment.

2. Nanocatalysts Preparation and Procedures

The Cr incorporated SAPO-34 catalysts were prepared by direct hydrothermal method from synthesis gels containing chromium species as active phase. The molar composition of synthesis gel to prepare direct-hydrothermally synthesized CrAPSO-34 with different Cr content was 2TEAOH: $1Al_2O_3$: $0.3SiO_2$: yCr_2O_3: $1P_2O_5$: $70H_2O$ (y: 0, 0.005, 0.05). Typically, a required amount of aluminum tri isopropylate was dissolved in TEAOH under vigorous stirring for 90 min at room temperature. Chromium nitrate was added to the homogeneous mixture followed by fumed silica. Stirring was continued for another 1 h until the mixture was homogeneous. Finally, phosphoric acid was added dropwise and the resulting mixture was stirred at room temperature moderately for 24 h. The crystal's nuclei were then allowed to grow by transferring the initial gel into a 90 ml Teflon-lined stainless steel autoclave and heating it in an oven at 200 °C for 72 h. The solid product was recovered and washed several times by sequential centrifuging with distilled water, and then dried overnight at 110 °C. The obtained powder was first calcined at 550 °C for 12 h to remove organic template completely and then calcined again at 700 °C in air for 4 h. The samples were denoted as CrAPSO-34(x), where x stands for the nominal Cr/Al molar ratio in the initial gel. For comparison, Cr supported SAPO-34 catalyst denoted as Cr/SAPO-34 was synthesized by wet impregnation of SAPO-34 with the required amount of aqueous chromium nitrate solution, corresponding to Cr content used in the initial gel of CrAPSO-34(0.05) sample. After impregnation for 24 h, the material was dried at 110 °C for 12 h and finally calcined in air at 700 °C for 4 h. Details of the samples preparation are illustrated in Fig. 1.

3. Nanocatalysts Characterization

X-ray diffraction (XRD) was employed to identify the compounds and verify the crystalline structure of nanocatalysts. It was carried out on a D-5000, Siemens diffractometer employing Cu-Ka radiation coupled to an X-ray tube operated at 30 kV, 40 mA and the scanning range of 2θ=8-90°. The morphology and particle size of the nanostructure catalysts were observed by field emission scanning electron microscopy (FESEM) analyzer (HITACHI S-4160). The samples studied were covered with a thin film of gold (ion sputtering) to improve conductivity. To study the morphology and dispersion of the supported chromium species, transmission electron microscopy (TEM) analysis was carried out using a Philips CM-200 electron microscope operated at 150 kV. Samples were ultrasonically dispersed in ethanol and then a drop of the suspension was put on a thin carbon film-coated Cu grid. Energy dispersive X-ray analysis (EDX) was carried out by MIRAPLMU for elemental analysis. The specific surface area of the samples was computed from N_2 adsorption result using a surface area analyzer (Quantachrome ChemBET-3000) according to the BET equation. Before analysis, all samples were degassed at 200 °C for 30 min.

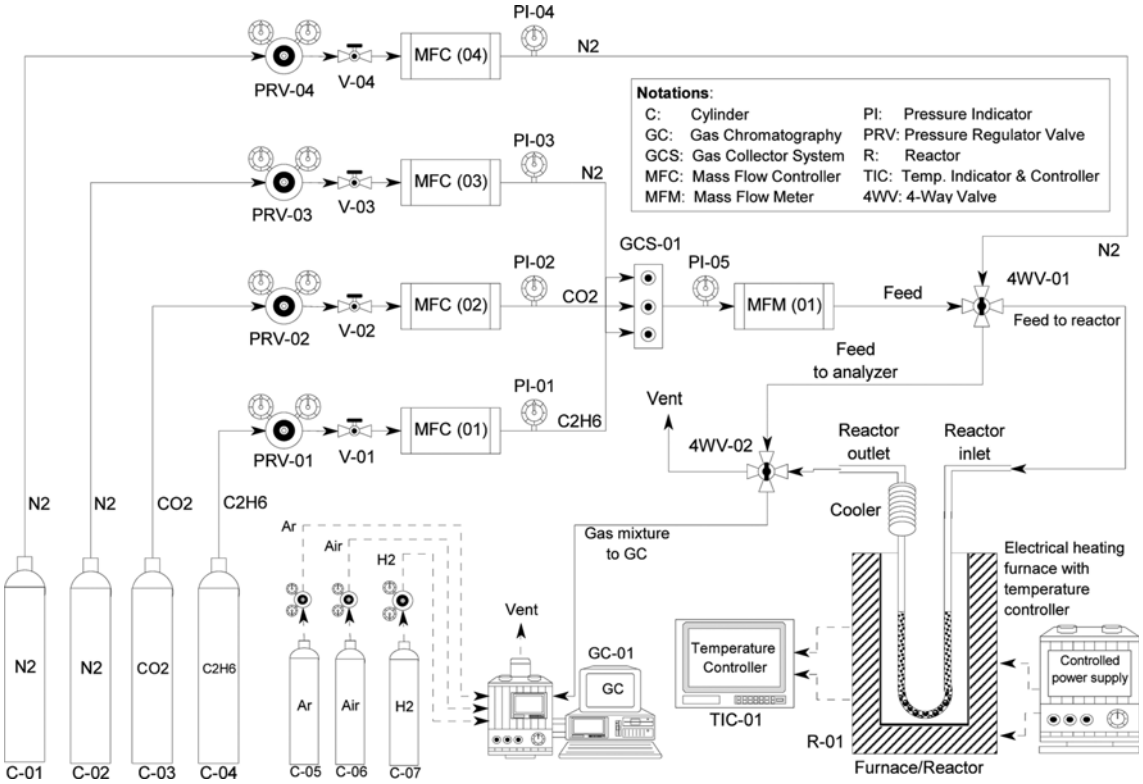

Fig. 2. Experimental setup for testing of catalytic performance of synthesized nanostructured catalysts used in C_2H_6/CO_2 oxidative dehydrogenation reaction.

The process of N_2 uptake and N_2 desorption was at −196 °C and room temperature, respectively. Catalyst acidity was measured by ammonia temperature programmed desorption (NH_3-TPD) using BELCAT analyzer equipped with a TCD detector. Prior to analysis, 0.1 g of calcined sample was preheated at 550 °C for 1 h in a He flow (50 cm^3/min) and then cooled to 100 °C. Ammonia adsorption was made from an NH_3/He gas mixture containing 5% (molar basis) ammonia with total flow rate of 50 cm^3/min at 100 °C. Afterwards, the samples were kept under a helium gas flow at 100 °C to remove physically adsorbed NH_3 molecules. Finally, the helium flow (50 cm^3/min) was passed through the sample with raising temperature up to 800 °C at a rate of 10 °C/min. For addressing surface functional groups, Fourier transform infrared spectroscopy (FTIR, UNICAM 4600) was done in the range of 400-4,000 cm^{-1} wave number. A self-supported wafer containing 10 wt% of KBr was used.

4. Nanocatalysts Performance Test

Fig. 2 illustrates the experimental setup for catalytic evaluation of synthesized samples. The catalytic measurements were performed in a fixed-bed quartz reactor (6 mm i.d.) packed with 500 mg of the catalyst. The catalyst particles were diluted with quartz chips to achieve isothermal operation and to keep constant volume in the catalytic bed. The catalytic bed was sandwiched between two layers of quartz sand to fix it, to ensure proper distribution of fluid flow, and to homogenize the feed temperature. The reactor was placed inside an electrical furnace which provided the required temperature for catalytic reaction. Catalytic reactions were at temperatures ranging from 600 to 700 °C with a reactant flow rate of 50 ml/min and at atmospheric pressure under steady-state conditions. For dehydrogenation of ethane in the presence of CO_2, the gas reactant contained 10 vol% ethane, 50 vol% CO_2, and the balance nitrogen, while in the absence of CO_2, the dehydrogenation feed consisted of 10 vol% ethane and the balance nitrogen. Prior to each catalytic test, the catalyst was first activated in situ at T= 600 °C for at least 0.5 h under 15 cm^3 min^{-1} of an air flow to remove any trace of water or inorganic compounds physisorbed on the surface and also to keep the catalyst oxygen level as high as possible. Afterwards, the air flow was switched to reaction feed and the catalyst was maintained at this temperature for 20 min before starting analysis. The reactants and products were analyzed on-line by a gas chromatograph (GC Chrom, Teif Gostar Faraz, Iran) equipped with TCD and FID detectors and a Carboxen-1000 column (Agilent Co.). Before analysis, the effluent stream was passed through an ice-cooled trap to condensate and separate H_2O. Blank tests performed under the same experimental conditions excluded the occurrence of homogenous reactions.

The ethane conversion, the ethylene yield and selectivity were calculated as follows:

$$X_{C_2H_6}\% = 100 \times \frac{(F_{C_2H_6})_{in} - (F_{C_2H_6})_{out}}{(F_{C_2H_6})_{in}} \quad (1)$$

$$S_{C_2H_4}\% = 100 \times \frac{F_{C_2H_4}}{(F_{CH_4} + F_{C_2H_4})} \quad (2)$$

$$Y_{C_2H_4}\% = 100 \times \frac{F_{C_2H_4}}{(F_{C_2H_6})_{in}} \quad (3)$$

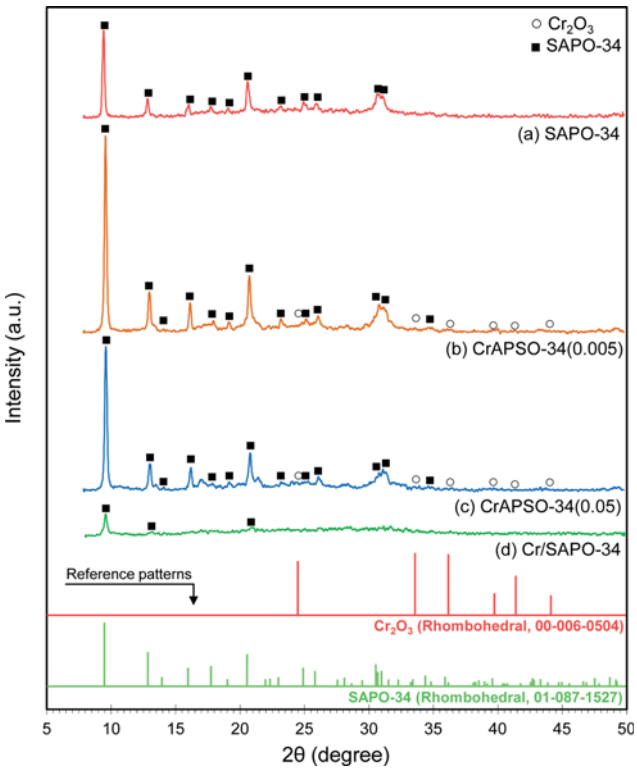

Fig. 3. XRD patterns of synthesized nanostructured catalysts: (a) SAPO-34, (b) CrAPSO-34(0.005), (c) CrAPSO-34(0.05) and (d) Cr/SAPO-34.

where, F_i is the molar flow rate of each component. All the experimental data were collected after the reaction for 0.5 h.

RESULTS AND DISCUSSION

1. Nanocatalyst Characterization

1-1. XRD Analysis

XRD patterns of parent SAPO-34 and chromium-based catalysts are shown in Fig. 3. It is evident that the Cr incorporated SAPO-34 samples have a typical CHA crystalline structure (JCPDS: 01-087-1527), in agreement with that of SAPO-34 reported in the literature [27,28]. The patterns indicated high crystallinity without any impurity. As can be seen, CrAPSO-34s show higher crystallinity compared to the parent SAPO-34 sample, reflecting higher nucleation rate in the presence of metal heteroatoms. Qualitatively, the crystallinity of the CrAPSO-34 samples varied depending on the Cr content used in the initial gel. It exhibited first an increasing, then a decreasing trend with gradually increasing Cr content in initial gel. As given in Table 1, the relative crystallinity of SAPO-34, CrAPSO-34(0.005) and CrAPSO-34(0.05) catalysts was 43.2, 100 and 72.1%, respectively. Crystallinity loss by further increasing Cr amount may be addressed by the appearance of extra-framework chromium and silicon species. From this observation, it can be speculated that SAPO-34 probably contaminated with amorphous phase when chromium content was more than 0.005, which can be supported by the FESEM and BET analysis. In addition, high thermal stability of the directly synthesized samples can be

Table 1. Structural and textural properties of nanostructured Cr incorporated/supported SAPO-34 samples

Sample	Synthesis method	Relative crystallinity[a] (%)	S_{BET} (m^2/g)
SAPO-34	Hydrothermal	43.2	463.3
CrAPSO-34(0.005)	One-pot hydrothermal	100	496.1
CrAPSO-34(0.05)	One-pot hydrothermal	72.1	472.4
Cr/SAPO-34	Hydrothermal/Impregnation	10.4	214.7

[a]Relative crystallinity: relative intensity of XRD patterns at 2θ=9.4°

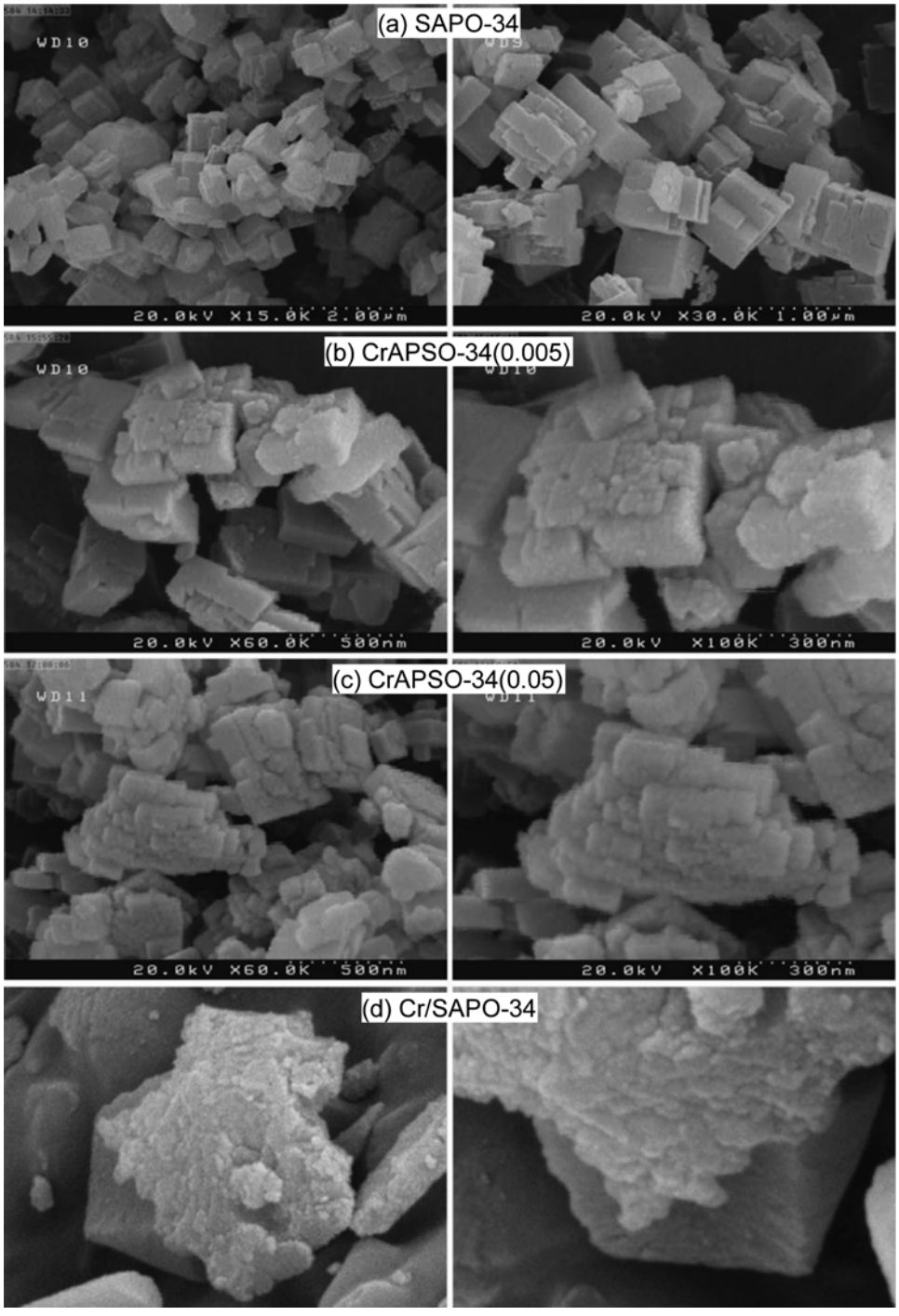

Fig. 4. FESEM images of synthesized nanostructured catalysts: (a) SAPO-34, (b) CrAPSO-34(0.005), (c) CrAPSO-34(0.05) and (d) Cr/SAPO-34.

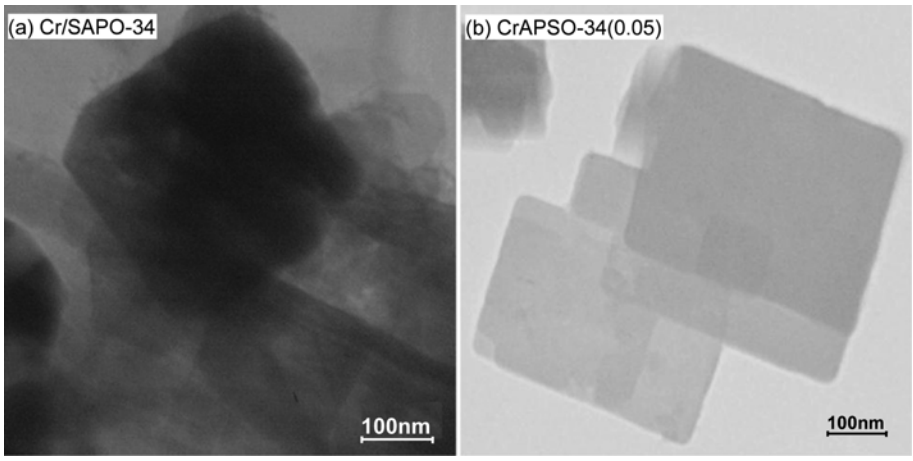

Fig. 5. TEM images of synthesized nanostructured catalysts: (a) Cr/SAPO-34 and (b) CrAPSO-34(0.05).

clearly realized by the observation of all characteristic peaks of SAPO-34. Regarding the literature [29], well-organized SAPO-34 structure is usually stable upon removal of the organic template and has been found to exhibit thermal stability nearly up to 1,100 °C. The identification of the major characteristic peaks, centered at 2θ=9.4, 12.9 and 20.5° in spite of weak intensity, confirmed the SAPO-34 presence in the crystalline structure of Cr supported SAPO-34 catalyst. However, substantial decrease of intensity was observed and relative crystallinity dropped to 10.4%. This observation can be interpreted by the support coverage upon Cr loading, as could be realized from BET, TEM and SEM results presented as follows. Detection of SAPO-34 as the only crystalline phase and absence of diffraction line of α-Cr_2O_3 in the structure of Cr-based SAPO-34 samples can be explained by highly dispersion of Cr species and/or the low amount of Cr-loading. However, for CrAPSO-34(0.005), low Cr content is mainly responsible. Note that the presence of α-Cr_2O_3 has a negative effect on the catalytic activity due to the poor accessibility of lattice chromium entities in the bulk of α-Cr_2O_3 [5,13,30]. Moreover, crystalline α-Cr_2O_3 is highly resistant to oxidant which makes it useless as a catalyst [13,30].

1-2. FESEM Analysis

FESEM images shown in Fig. 4 demonstrate the morphology of the parent SAPO-34 and chromium-containing SAPO-34 catalysts. The cubic rhombohedra structure, which is typical of SAPO-34 molecular sieves [31,32], can be clearly identified for all directly synthesized samples confirming the corresponding XRD analysis. The presence of Cr heteroatoms in the precursors' solution not only resulted in any distribution of the SAPO-34 framework, but also decreased the particle size. Some morphological changes of synthesized samples, brought about by variation of chromium content in the SAPO-34 framework, are easily distinguished. As Cr content rose from 0.005 to 0.05, much rougher and smaller crystals appeared. In fact, the crystals contaminated with irregular particles confirming the corresponding XRD analysis in which CrAPSO-34(0.05) exhibits a loss of crystallinity in comparison with CrAPSO-34(0.005). Appearance of the irregular particles and absence of any XRD peak of other crystalline phase indicated that they were amorphous phase. Crystal size and uniformity and surface smoothness show decreasing trend with increasing the chromium content. Comparing the FESEM images of Cr supported SAPO-34 (Cr/SAPO-34) with those of Cr incorporated SAPO-34 sample with the same Cr content reflects the remarkable effect of deposition method on the surface morphology. As seen, by chromia loading, fine nanoparticles and agglomerations were formed over the SAPO-34 structure covering the support surface and so changing the surface morphology. These results reflect that impregnation method cannot guarantee complete spreading of the Cr species. Accordingly, it is expected that the Cr supported SAPO-34 sample exhibits low surface area, which is going to be supported by the BET analysis.

1-3. TEM Analysis

Fig. 5 displays the TEM images of the Cr/SAPO-34 and CrAPSO-34(0.05) catalysts. The small dark spots are attributed to the deposited chromium oxides nanoparticles, and the faint background represents the SAPO support. As can be seen from TEM image of the CrAPSO-34(0.05) sample, no chromium oxides appear on the external surface of the cubic SAPO particles. This is the supporting evidence for the presence of more chromium species in the SAPO-34 framework. In contrast, almost vast, dark regions can be clearly evidenced for the TEM image of the nanostructured Cr/SAPO-34 catalyst, suggesting the coverage of a sight of the SAPO-34 external surface by Cr species. This conclusion is in good agreement with the FESEM and XRD results stated above. This can be justified by considering the Cr loading method and textural and structural characteristics of SAPO materials. Considering the above, it is reasonable to conclude that the one-pot hydrothermal can partly reduce the restriction of attainable chromium loading in preparing Cr-based catalysts supported on SAPO-34.

1-4. EDX Analysis

It is well known that the dispersion of chromium species is a major factor affecting the intrinsic activity of Cr containing catalysts in the oxidative dehydrogenation process. To determine the elemental composition and also assess the dispersion of Cr species in the synthesized samples, the EDX analysis was carried out. The EDX micrographs including spectrums and dot-mappings are shown in Fig. 6. Only Al, P, Si and Cr elements were detected, confirming the presence of all elements used in the synthesis of all

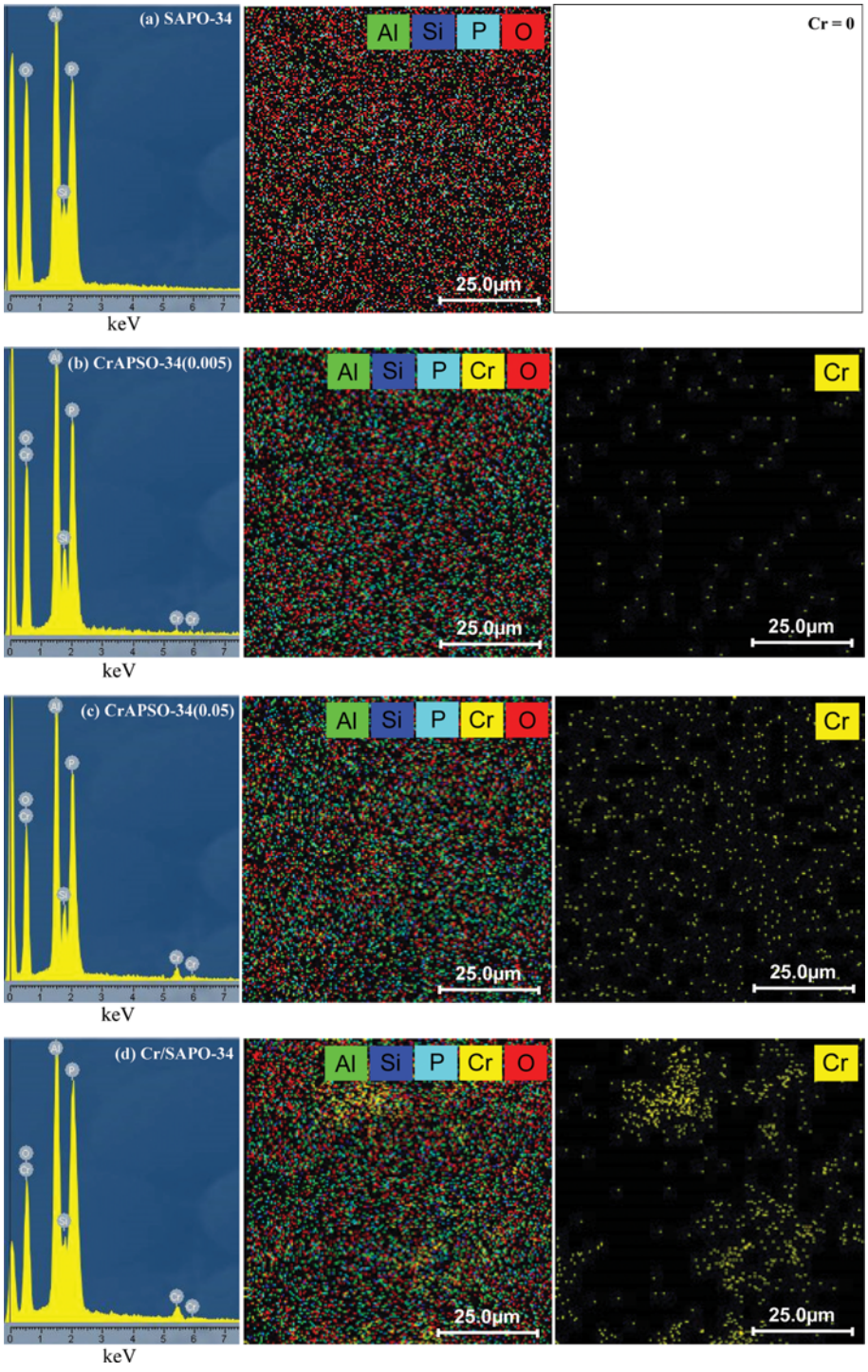

Fig. 6. EDX analysis of synthesized nanostructured catalysts: (a) SAPO-34, (b) CrAPSO-34(0.005), (c) CrAPSO-34(0.05) and (d) Cr/SAPO-34.

samples and absence of any impurities in their structure. Interestingly, the composition of directly synthesized samples obtained by the EDX spectra and the corresponding initial gel, given in Table 2, are close to each other. This is additional evidence for the successful synthesis and, more importantly, the ability of one-pot hydrothermal synthesis method to uniformly disperse Cr species. Although the Si/Al ratio in the starting gels of all catalysts is constant and equal to 0.3, the Si/Al ratio of CrAPSO-34(0.05) was found to be lower than this value after crystallization. EDX results indicate that a lower amount of silicon is incorporated into the SAPO-34 framework. It is indicative of decreasing the capability of the crystallite framework to incorporate Si by increasing Cr content in the initial gel. By taking the fact into account that structural hydroxyls as strong Brønsted acid sites are generated by Si incorporation, it is reasonable to expect lower number of moderate acid sites compared to SAPO-34, which is going to be sup-

Table 2. Surface chemical analysis of nanostructured Cr incorporated/supported SAPO-34 samples

Sample	Gel composition (wt%)				Catalyst composition (wt%)				Si/Al (mol/mol)	
	Al	Si	P	Cr	Al	Si	P	Cr	Gel	Catalyst
SAPO-34	40.66	12.65	46.69	0	45.06	13.88	41.07	0	0.3	0.296
CrAPSO-34(0.005)	40.51	12.60	46.50	0.39	43.56	13.78	41.94	0.72	0.3	0.304
CrAPSO-34(0.05)	39.13	12.17	44.93	3.78	43.71	11.93	40.33	4.04	0.3	0.262
Cr/SAPO-34	39.13	12.17	44.93	3.78	40.40	12.34	40.19	7.07	0.3	0.293

ported by TPD analysis. Regarding FESEM findings, a high degree of Cr dispersion was expected for direct-hydrothermally synthesized catalysts. The apt dispersion of chromium in the EDX dot-mapping results of Cr incorporated SAPO-34 samples confirms this expectancy. Moreover, the comparison between the Cr based samples including Cr incorporated SAPO-34 and Cr supported SAPO-34 with the same chromium loading reveals that, one-pot hydrothermal method enables an extremely uniform dispersion of Cr species on the surface, which is going to affect the catalytic process. Besides, this uniformity can strongly reduce the typical inhomogeneity of heterogeneous catalysts.

1-5. BET Analysis

One of the most influential parameters of the heterogeneous catalysts is their specific surface area. Higher surface area facilitates the reactants adsorption step and provides more redox Cr species, which are responsible for enhancing the catalytic performance. The calculated total specific surface areas (SSA) for prepared samples are listed in Table 1. The examination of obtained results reveals that upon the addition of Cr species to SAPO molecular sieves, the surface area altered depending on deposition method and also metal content employed in the synthesis route. All the direct-hydrothermally synthesized samples exhibited high surface area (400-500 m^2/g), representing the capability of one-pot hydrothermal method in the synthesis of SAPO-34-containing catalysts. A measurable increase of surface area was found by Cr incorporation into SAPO-34 framework, which can be associated with decrease of cubic particles size. Moreover, it is well believed that parent and modified SAPO-34 material with higher crystallinity exhibits higher surface area [31,33]. A slight expansion in the unit cell volume as a result of the probably replacement of Al^{3+} by Cr^{3+} in the tetrahedral SAPO-34 framework could be another reasonable explanation for this observation. As expected, the results clearly show a similar trend to that observed for crystallinity of Cr incorporated SAPO-34 with increasing chromium content. It can be seen that increasing Cr content in the initial gel from 0.0 to 0.005 leads to the rises in the surface area from 463.3 to 496.1 m^2/g. However, with the continued increase of the Cr content up to 0.05, the surface area declined to 472.4 m^2/g. It is reasonable to attribute this decreasing trend to probably the presence of extra-framework species and amorphous phase formation, in accordance with FESEM images. As seen, Cr supported SAPO-34 sample has much smaller surface area in comparison with even the respective bare support. This decrease implies the penetration of chromium species into micropores and their deposition on the external surface of SAPO-34, which partially blocks the pores and channels. The TEM image and considerable loss of Cr/SAPO-34 crystallinity also support this hypothesis. The above results suggest that employing direct hydrothermal method in the synthesis of Cr-based catalyst containing SAPO-34 could be beneficial.

1-6. TPD-NH_3 Analysis

The acidic property is of significant importance in terms of ethane activation. Acidity of Cr-based catalysts could be varied through deposition method. TPD-NH_3 profiles and acidity data of SAPO-34 and Cr incorporated/supported SAPO-34 catalysts are shown in Fig. 7. Two desorption peaks, centered around 180-185 and 385-425 °C, corresponding to the weak and moderate acid sites appear for the synthesized samples, respectively. The free hydroxyl groups (i.e., SiOH) and the bridging hydroxyl groups are responsible for the weak and moderate acidity of these materials, respectively [31,33]. Regarding the presence of only weak to moderated acidic sites, high ethylene selectivity can be expected. Moreover, the result indicated that Cr incorporation into SAPO-34 framework led to an increase and decrease in the number of weak and mild acid sites, respectively. This could be well explained on the basis of decrease of Si incorporation amount and silicon islands

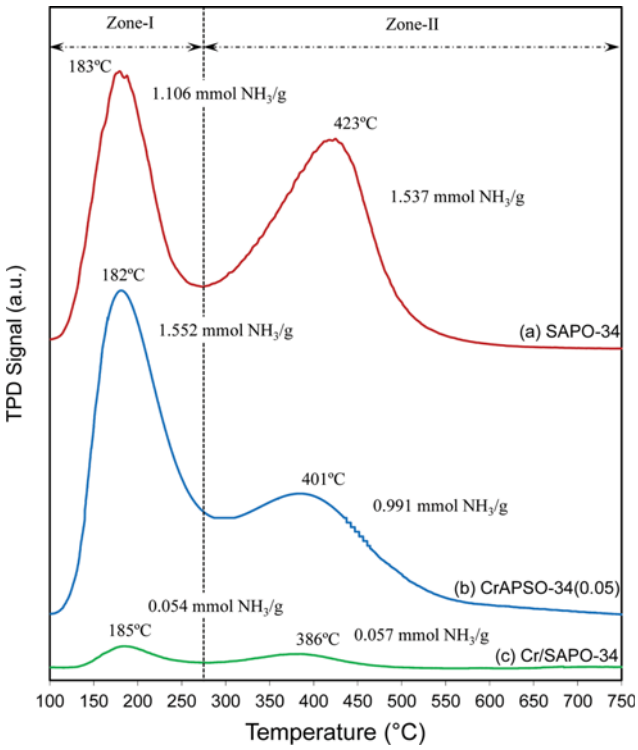

Fig. 7. TPD-NH_3 analysis of synthesized nanostructured catalysts: (a) SAPO-34 (b) CrAPSO-34(0.05) and (c) Cr/SAPO-34.

formation by rising Cr content as evidenced by EDX and FESEM results. Nevertheless, the number of total acid sites of SAPO-34 did not markedly change by Cr incorporation. By comparing TPD-NH_3 profiles of CrAPSO-34(0.05) with those of Cr/SAPO-34 sample with the same Cr content, it can be found that the one-pot hydrothermal method endows the catalyst with much higher acidity in number. Upon Cr loading over SAPO-34 by impregnation method, the number of acid sites considerably decreased. It is obvious that the blocking of acidic sites by the chromium species is responsible for the substantial decrease in the surface acidity of nanostructured Cr/SAPO-34 catalyst. This is another supporting evidence for the surface coverage in Cr supported SAPO-34 sample, which is in good agreement with the XRD, BET and FESEM results. Considering the above, one could expect that Cr incorporated SAPO-34 nanostructured catalyst exhibits superior performance for the CO_2-assissted dehydrogenation of ethane.

1-7. FTIR Analysis

FTIR spectra of the as-synthesized samples are shown in Fig. 8. The vibration frequency peaks at 420, 490, 640, 710, 1,100, 1,400, 1,640, 2,350 and 3,450 cm^{-1} can be recognized from absorption spectra of the prepared samples, which are the typical vibrations in SAPO-34 based samples [34-36]. The same bonds were present in the structure of all samples, though with different concentrations. The IR bands detected at 420 cm^{-1} in the spectrum corresponded to M-O stretching vibrations [37,38]. Based on the literature assignments, the absorption bands appearing around 490, 640, 710 and 1,100 cm^{-1} are assigned to the characteristic vibration peaks of the SAPO-34 phase [31,33,39]. In detail, the peak at 490 cm^{-1} can be attributed to the bending vibration of PO_4, AlO_4 and SiO_4 [40-42]. IR bands around 640, 710, 1,100 cm^{-1} are ascribed to the T-O bending in D-6 rings, asymmetric and symmetric vibrations of O-P-O, respectively [31-33,39]. The bands around 1,100 cm^{-1} can also be attributed to M-OH stretching vibrations [38,43,44]. The absence of IR peak around 610 cm^{-1} which is a characteristic for α-Cr_2O_3 phase of chromium oxide [37,38] seems to discard the presence of Cr_2O_3 crystallites in the structure of Cr containing materials and thus supporting the XRD results. Moreover, the absorption bands appearing around 1,400 and 1,640 cm^{-1} can be assigned to physically adsorbed water on the catalysts surface which occurred during maintenance of synthetic samples [45-48]. The weak peak observed at 2,350 cm^{-1} corresponds to the asymmetric stretching frequency [υ(CO)] of CO_2, which can be addressed by the adsorption of aerial CO_2 over the course of FTIR analysis [49-51]. The strong broad peaks in the range of 3,000-3,700 cm^{-1} arise from the free and bridging hydroxyls vibration [20,21,31-33]. The bridging hydroxyls, i.e. -SiOHAl-, are considered to be the active sites for oxidative dehydrogenation (ODH) reaction, while free hydroxyls (P-OH, Al-OH and Si-OH) might be also involved in ODH reactions run at high temperatures [20,21]. Absorbance at 3,000-3,700 cm^{-1} in the spectrum of CrAPSO-34(0.05) qualitatively seems to be stronger than that of Cr supported SAPO-34 one as an evidence for higher efficient active sites. The resulting trend in the hydroxyls concentration was found to be consistent with the TPD findings. By Cr impregnation over SAPO-34, the intensity of related peaks strongly declined. It is reasonable to attribute this reduction to the surface coverage by Cr species loading, in accordance with FESEM and TEM images, XRD, BET and NH_3-TPD results. Besides, the presence of OH groups due to their ability in removing the formed coke is also very noticeable [52]. By taking these features into consideration, it seems that superior performance of CrAPSO-34(0.05) catalyst is somewhat related to the higher intensity of OH groups compared to Cr/SAPO-34 catalyst.

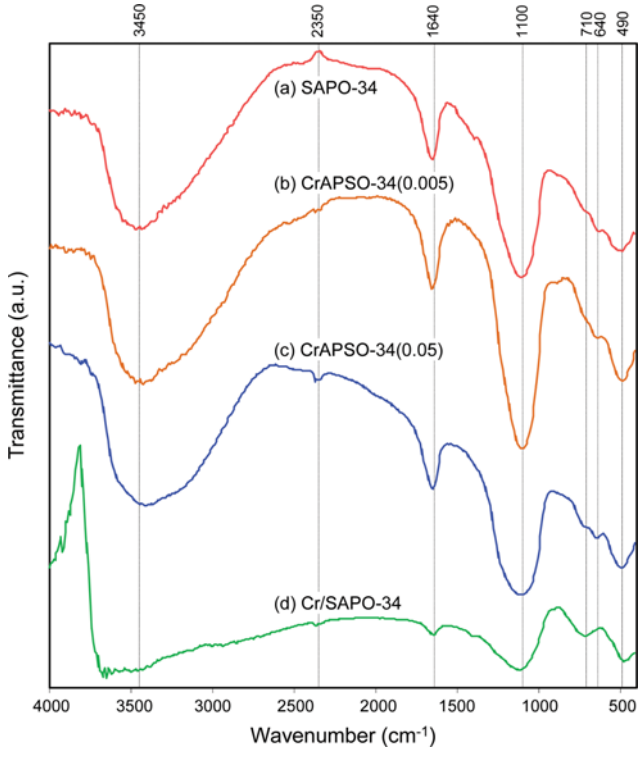

Fig. 8. FTIR spectra of synthesized nanostructured catalysts: (a) SAPO-34, (b) CrAPSO-34(0.005), (c) CrAPSO-34(0.05) and (d) Cr/SAPO-34.

2. Catalytic Performance Toward C_2H_6/CO_2 Oxidative Dehydrogenation

2-1. Effect of Catalyst on C_2H_6 Conversion and C_2H_4 Yield

The catalytic activity of the synthesized Cr containing SAPO-34 catalysts in the ethane dehydrogenation with CO_2 was evaluated in terms of C_2H_6 conversion and ethylene yield at temperatures ranging from 600 to 700 °C and shown in Fig. 9. The equilibrium conversions were also calculated from the thermodynamic estimation of the process described in literature [2]. As can be seen, the conversion values obtained don't exceed the equilibrium conversions, intended as an upper limit with respect to the non-equilibrium conditions attained in the tests, verifying the authenticity of the measured data. The catalytic performance of the samples is found to be strongly dependent on the reaction temperature. Over all examined samples, both the ethane conversion and ethylene yield increase with the rise of the reaction temperature owing to the endothermic nature of ODH in the presence of CO_2. This is in accordance to the thermodynamic study of the process. From the variation of catalytic activity with reaction temperature, it can be deduced that the catalysts are more active at higher temperature. The best performance obtained at 700 °C for all the examined samples. In addition, the ethane conversion and the ethylene yield

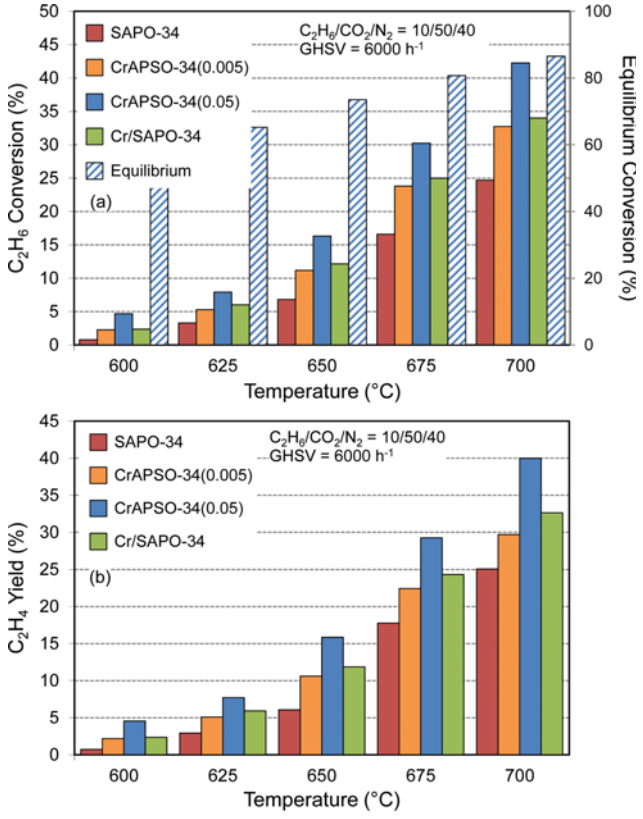

Fig. 9. Effect of catalyst type and temperature on (a) C_2H_6 conversion and (b) C_2H_4 yield.

are close to each other in whole temperature range, showing high ethylene selectivity. This can be ascribed to the soft oxidant applied and favorable acidity properties of SAPO materials. Moreover, these results clearly indicate that the chromium content and deposition method also play a decisive role in determining the catalytic activity. As expected, ethane conversion and ethylene yield of directly synthesized samples remarkably enhance upon the Cr loading and also by increasing its content. The enhanced activity of Cr incorporated SAPO-34 catalysts compared to bare SAPO-34 confirms the positive role played by Cr in facilitating ethane activation. The highest performance amongst the directly prepared catalysts was observed with CrAPSO-34(0.05), which is related to more amount of Cr species as active phase. The catalyst displayed an ethane conversion of 42.2% and 40% ethylene yield at 700 °C. Compared to Cr/SAPO-34 catalyst, CrAPSO-34(0.05) exhibits better catalytic activity, indicating promoting effect of one-pot method on the catalytic activity. This enhancement could be explained by better chromium species dispersion over the SAPO-34 framework with well-organized three-dimensional pore structure, higher surface area, more acid sites and higher concentration of OH groups evidenced by EDX dot-mapping, BET, TPD and FTIR analysis, respectively.

2-2. Effect of GHSV on Catalytic Performance

To clarify the contact time impact, the catalytic activity of the most effective catalyst, CrAPSO-34(0.05), was studied as a function of reaction temperature at various weigh hourly space velocities (GHSVs) and obtained results were depicted in Fig. 10. The

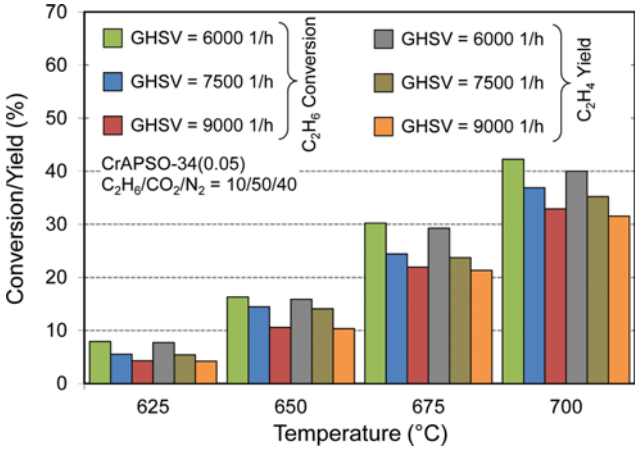

Fig. 10. Effect of GHSV on C_2H_6 conversion and C_2H_4 yield: CrAPSO-34(0.05).

space velocity was varied by increasing the feed rate. It is customary to anticipate lower ethane conversion and ethylene yield at higher space velocities. These results clearly indicate that upon increasing the space velocity, both the conversion and yield declined for all the examined temperatures. A plausible explanation to this behavior could be related to the decrease of reactants residence time with rise in space velocity which lowers the catalytic activity. As seen, even with increasing GHSV by 50%, reasonable activity toward catalytic oxidative dehydrogenation of ethane is still achieved.

2-3. Effect of CO_2 Addition on Catalytic Performance

Depending on the nature of catalyst used, CO_2 exhibits promoting or poisoning effect on catalytic performance in the dehydrogenation process [7,8,13,53]. To elucidate the CO_2 effect, the dehydrogenation of ethane in the CO_2 atmosphere was compared with that in the inert N_2 atmosphere over CrAPSO-34(0.05) catalyst, as depicted in Fig. 11. Clearly, in the CO_2 atmosphere, the ethane conversion and ethylene yield are higher than those in the N_2 atmosphere. The selectivity to ethylene in CO_2 (not shown here) is also higher than that in N_2 (generally higher than 90% in both atmospheres). These results clearly demonstrate that CO_2 plays a favor-

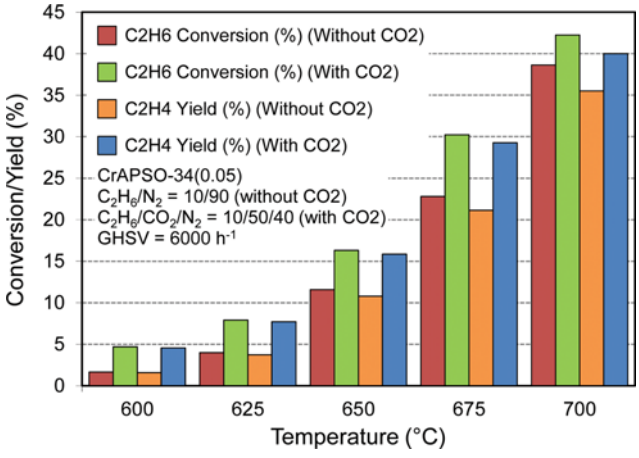

Fig. 11. Effect of CO_2 addition and temperature on C_2H_6 conversion and C_2H_4 yield: CrAPSO-34(0.05).

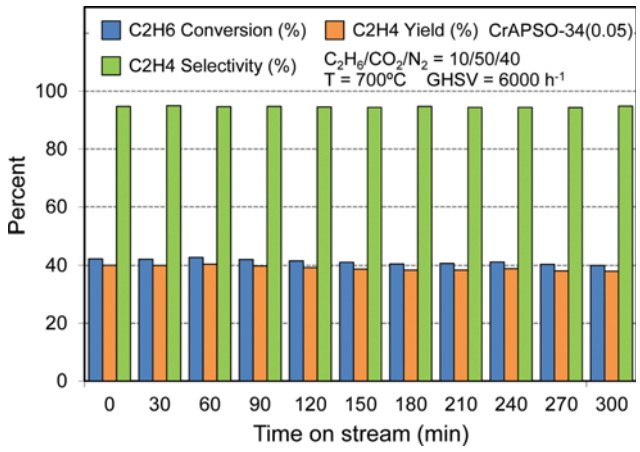

Fig. 12. Time on stream behavior of CrAPSO-34(0.05).

able role in the ODH of ethane reaction. CO_2 serves as a mild oxidant in the case of redox oxides, which can generate active oxygen species facilitating ethane dehydrogenation [4,5,13]. Generally, the reduction of the carbon deposition, the assistant in the rapid desorption of olefins from the catalyst surface, re-oxidation of reduced active species and poisoning the non-selective sites have been mainly proposed as some possibilities for explaining the promoting effect of CO_2 on the dehydrogenation of light alkanes over several catalysts in the literature [2,14,54,55].

2-4. Time on Stream Performance

High stability, together with the superior activity, is the characteristic of a promising catalyst used in the oxidative dehydrogenation of ethane with CO_2. Accordingly, the best catalyst (CrAPSO-34(0.05)) was evaluated continuously for 5 h under the optimum reaction conditions, as shown in Fig. 12. No obvious change has been observed in the catalytic performance up to 5 h, implying less sensitivity of catalyst to deactivation during the course of running the reaction. As known, both the coke formation and reduction of redox Cr species contribute to the deactivation of dehydrogenation catalysis [4,5,10,14,56]. It is plausible to attribute this long-term stability to high concentration of acid sites, high surface area and extremely uniform dispersion of metal evidenced by TPD, BET and EDX dot-mapping analysis, respectively. Less carbon being formed during reaction owing to low to moderate surface acidity and high concentration of surface hydroxyl groups, reinforcement of metal-support interaction and thereupon, stabilization of the oxidation states of Cr species as a result of incorporating metal into framework and enhanced dispersion; and also the regeneration of active sites with CO_2 in the feed may be other reasons.

CONCLUSIONS

The results reflect that the structural properties of catalysts and their catalytic performance are strongly dependent on the Cr content and deposition method. With an increase in the incorporated Cr content, smaller cubic crystals and amorphous particles were obtained, leading to a decrease of the surface area and crystallinity of Cr rich catalyst. However, the extra-framework species probably appeared with gradually increasing Cr content in initial gel. On the other hand, Cr loading by wet impregnation route led to micropore blockage and surface coverage and, thereupon, substantial decrease of the surface area and acidity while well-organized CHA structure of the support was retained upon the chromium incorporation as evidenced by XRD, FESEM and BET analysis. Therefore, high surface area was obtained on the final catalyst. In fact, Cr incorporation not only preserved but also promoted the crystalline framework of SAPO-34, resulting in higher surface area of Cr incorporated SAPO-34 catalyst contrary to Cr supported SAPO-34 one. Moreover, direct synthesis allowed more effective surface acidity and extremely uniform chromium dispersion to be achieved, features that account for superior catalytic performance and stability of directly synthesized Cr rich catalyst. Simplicity of preparation and less synthesis cost and time are other advantages. The catalyst effectively dehydrogenated ethane to ethylene in the presence of CO_2 at 700 °C even after 5 h on-stream operation, giving 40 and 94.8% ethane conversion and ethylene selectivity, respectively. According to these findings, it can be concluded that the Cr incorporated SAPO-34 material is an attractive catalyst applicable for ethane dehydrogenation to ethylene with CO_2. Besides, the one-pot hydrothermal method can be applied as a promising approach to efficiently synthesize the Cr-based catalysts.

ACKNOWLEDGEMENTS

The authors gratefully acknowledge Sahand University of Technology for the financial support of the project as well as Iran Nanotechnology Initiative Council for complementary financial support.

REFERENCES

1. A. J. R. Castro, S. P. D. Marques, J. M. Soares, J. M. Filho, G. D. Saraiva and A. C. Oliveira, *Chem. Eng. J.*, **209**, 345 (2012).
2. M. A. Botavina, G. Martra, Y. A. Agafonov, N. A. Gaidai, N. V. Nekrasov, D. V. Trushin, S. Coluccia and A. L. Lapidus, *Appl. Catal. A: Gen.*, **347**, 126 (2008).
3. S. Deng, S. Li, H. Li and Y. Zhang, *Ind. Eng. Chem. Res.*, **48**, 7561 (2009).
4. P. Michorczyk, J. Ogonowski and M. Niemczyk, *Appl. Catal. A: Gen.*, **374**, 142 (2010).
5. P. Michorczyk, P. Pietrzyk and J. Ogonowski, *Micropor. Mesopor. Mater.*, **161**, 56 (2012).
6. N. Mimura, I. Takahara, M. Inaba, M. Okamoto and K. Murata, *Catal. Commun.*, **3**, 257 (2002).
7. T. Shishido, K. Shimamura, K. Teramura and T. Tanaka, *Catal. Today*, **185**, 151 (2012).
8. I. Takahara, W. C. Chang, N. Mimura and M. Saito, *Catal. Today*, **45**, 55 (1998).
9. R. X. Valenzuela, G. Bueno, A. Solbes, F. Sapina, E. Martínez and V. Cortés Corberan, *Topics in Catal.*, **15**, 181 (2001).
10. F. Zhang, R. Wu, Y. Yue, W. Yang, S. Gu, C. Miao, W. Hua and Z. Gao, *Micropor. Mesopor. Mater.*, **145**, 194 (2011).
11. H. Liu, Z. Zhang, H. Li and Q. Huang, *J. Natural Gas Chem.*, **20**, 311 (2011).
12. P. Michorczyk, J. Ogonowski, P. Kuśtrowski and L. Chmielarz,

Appl. Catal. A: Gen., **349**, 62 (2008).
13. P. Michorczyk, J. Ogonowski and K. Zeńczak, *J. Mol. Catal. A: Chem.*, **349**, 1 (2011).
14. X. Shi, S. Ji and K. Wang, *Catal. Lett.*, **125**, 331 (2008).
15. T. Blasco and J. M. L. Nieto, *Appl. Catal. A: Gen.*, **157**, 117 (1997).
16. M. Setnička, R. Bulánek, L. Čapek and P. Čičmanec, *J. Mol. Catal. A: Chem.*, **344**, 1 (2011).
17. M. Piumetti, B. Bonelli, P. Massiani, S. Dzwigaj, I. Rossetti, S. Casale, M. Armandi, C. Thomas and E. Garrone, *Catal. Today*, **179**, 140 (2012).
18. L. M. Madeira and M. F. Portela, *Catal. Rev.*, **44**, 247 (2002).
19. V. D. B. C. Dasireddy, S. Singh and H. B. Friedrich, *Appl. Catal. A: Gen.*, **421-422**, 58 (2012).
20. L. Lisi, L. Marchese, H. O. Pastore, A. Frache, G. Ruoppolo and G. Russo, Topics *in Catal.*, **22**, 95 (2003).
21. L. Marchese, A. Frache, G. Gatti, S. Coluccia, L. Lisi, G. Ruoppolo, G. Russo and H. O. Pastore, *J. Catal.*, **208**, 479 (2002).
22. D. W. Flick and M. C. Huff, *Appl. Catal. A: Gen.*, **187**, 13 (1999).
23. Q. Zhu, J. N. Kondo, R. Ohnuma, Y. Kubota, M. Yamaguchi and T. Tatsumi, *Micropor. Mesopor. Mater.*, **112**, 153 (2008).
24. F. Bérubé, F. Kleitz and S. Kaliaguine, *J. Mater. Sci.*, **44**, 6727 (2009).
25. N. Rajic, D. Stojakovic, S. Hocevar and V. Kaucic, *Zeolites*, **13**, 384 (1993).
26. Z. Zhu, M. Hartmann and L. Kevan, *Chem. Mater.*, **12**, 2781 (2000).
27. J. Tan, Z. Liu, X. Bao, X. Liu, X. Han, C. He and R. Zhai, *Micropor. Mesopor. Mater.*, **53**, 97 (2002).
28. T. Wang, X. Lu and Y. Yan, *Micropor. Mesopor. Mater.*, **168**, 155 (2013).
29. L. Ye, F. Cao, W. Ying, D. Fang and Q. Sun, *J. Porous Mater.*, **18**, 225 (2011).
30. K. J. Wojciech and I. G. Dalla Lana, *J. Chem. Soc., Faraday Transactions*, **93**, 2583 (1997).
31. A. Izadbakhsh, F. Farhadi, F. Khorasheh, S. Sahebdelfar, M. Asadi and Y. Z. Feng, *Appl. Catal. A: Gen.*, **364**, 48 (2009).
32. G. Liu, P. Tian, Y. Zhang, J. Li, L. Xu, S. Meng and Z. Liu, *Micropor. Mesopor. Mater.*, **114**, 416 (2008).
33. A. Izadbakhsh, F. Farhadi, F. Khorasheh, S. Sahebdelfar, M. Asadi and Z. F. Yan, *Micropor. Mesopor. Mater.*, **126**, 1 (2009).
34. E. Aghaei and M. Haghighi, *J. Porous Mater.*, **22**, 187 (2015).
35. M. Charghand, M. Haghighi and S. Aghamohammadi, *Ultrasonics Sonochem.*, **21**, 1827 (2014).
36. E. Aghaei and M. Haghighi, *Micropor. Mesopor. Mater.*, **196**, 179 (2014).
37. T. Ivanova, K. Gesheva, A. Cziraki, A. Szekeres and E. Vlaikova, *J. Phys.: Conference Series*, **113**, 1 (2008).
38. H. R. Mahmoud, *J. Mol. Catal. A: Chem.*, **392**, 216 (2014).
39. G. Liu, P. Tian, J. Li, D. Zhang, F. Zhou and Z. Liu, *Micropor. Mesopor. Mater.*, **111**, 143 (2008).
40. F. Rahmani and M. Haghighi, *J. Natural Gas Sci. Eng.*, **27**, Part 3, 1684 (2015).
41. S. Aghamohammadi, M. Haghighi and M. Charghand, *Mater. Res. Bulletin*, **50**, 462 (2014).
42. F. Rahmani, M. Haghighi and M. Amini, *J. Ind. Eng. Chem.*, **31**, 142 (2015).
43. S. Allahyari, M. Haghighi, A. Ebadi and S. Hosseinzadeh, *Energy Conver. Manage.*, **83**, 212 (2014).
44. R. Khoshbin and M. Haghighi, *Chinese J. Inorganic Chem.*, **28**, 1967 (2012).
45. E. Aghaei and M. Haghighi, *Powder Technol.*, **269**, 358 (2015).
46. S. Aghamohammadi and M. Haghighi, *Chem. Eng. J.*, **264**, 359 (2015).
47. M. Charghand, M. Haghighi, S. Saedy and S. Aghamohammadi, *Adv. Powder Technol.*, **25**, 1728 (2014).
48. P. Sadeghpour and M. Haghighi, *Particuology*, **19**, 69 (2015).
49. D. Debasis and P. Panchanan, *J. Am. Ceramic Soc.*, **89**, 1014 (2004).
50. S. Mehdi Sajjadi, M. Haghighi, A. Alizadeh Eslami and F. Rahmani, *J. Sol-Gel Sci. Technol.*, **67**, 601 (2013).
51. M. Abdollahifar, M. Haghighi, A. A. Babaluo and S. Khajeh Talkhoncheh, *Ultrasonics Sonochem.*, **31**, 173 (2016).
52. M. A. Goula, A. A. Lemonidou and A. M. Efstathiou, *J. Catal.*, **161**, 626 (1996).
53. B. Xu, B. Zheng, W. Hua, Y. Yue and Z. Gao, *J. Catal.*, **239**, 470 (2006).
54. S. Chen, Z. Qin, G. Wang, M. Dong and J. Wang, *Fuel*, **109**, 43 (2013).
55. F. Urlan, I.-C. Marcu and I. Sandulescu, *Catal. Commun.*, **9**, 2403 (2008).
56. Q. Zhu, M. Takiguchi, T. Setoyama, T. Yokoi, J. Kondo and T. Tatsumi, *Catal. Lett.*, **141**, 670 (2011).